IEEE Access
Multidisciplinary | Rapid Review | Open Access Journal

Received March 3, 2021, accepted March 22, 2021, date of publication March 24, 2021, date of current version April 7, 2021.

Digital Object Identifier 10.1109/ACCESS.2021.3068617

Chromatic Dispersion Based Wide-Band, Fiber-Coupled, Tunable Light Source for Hyperspectral Imaging

GARGI SHARMA[1], SHEEZA KAINAT NAVEED[1,2], ASHA PARMAR[1], AND KANWARPAL SINGH[1,2]

[1]Max Planck Institute for the Science of Light, 91058 Erlangen, Germany
[2]Department of Physics, Friedrich-Alexander Universität Erlangen-Nürnberg, 91058 Erlangen, Germany

Corresponding author: Kanwarpal Singh (kanwarpal.singh@mpl.mpg.de)

ABSTRACT Hyperspectral imaging is a powerful label-free imaging technique that provides topological and spectral information at once. In this work, we have designed and characterized a hyperspectral source based on the chromatic dispersion property of off-the-shelf lenses and converted a supercontinuum laser light source into a hyperspectral imaging light source for 490 nm to 900 nm wavelength range with a spectral resolution of 3.5 nm to 18 nm respectively. The potential of the source was demonstrated by imaging two color dots with different absorption bands. Further, we generated the hypercube of the lily ovary and dense connective tissue and measured their spectral signature as a function of wavelength. We also imaged the lower tongue of a healthy volunteer at 540 nm, 630 nm, and white light. Our simple hyperspectral light source design can easily be incorporated in a standard endoscope or microscope to perform hyperspectral imaging.

INDEX TERMS Biomedical optical imaging, chromatic dispersion, hyperspectral imaging, light sources, spectroscopy.

I. INTRODUCTION

Optical microscopy has been a method of choice in the medical field for the topographical information of the tissue for more than 300 years [1]. Over the decades, researchers have been trying to improve disease diagnosis by developing and improvising different imaging techniques. In the field of biomedical imaging, microscopy can be broadly categorized into two parts; label-free and labeled imaging. For label-free imaging, the sample is illuminated with light and imaged using techniques such as wide-field microscopy, narrowband imaging [2], phase-contrast imaging [3], optical coherence tomography [4], X-ray computed tomography [5], magnetic resonance tomography [6], etc. Being less invasive, label-free imaging techniques are quite attractive compared to labeled imaging techniques but suffer from poor contrast. Labeled imaging techniques improve the imaging contrast by staining different parts of the sample with dyes and then imaging with techniques such as confocal microscopy [7] or fluorescence imaging [8]. Nevertheless, the quest to develop high contrast label-free imaging techniques is still on. Hyperspectral imaging (HSI) is one such technique that can achieve this ambitious goal by utilizing the inherent chromophores within a biological sample. HSI has existed for several decades [9]–[16] but only recently it has been applied in the biomedical field where it can prove as an intelligent tool for identifying anomalies in the tissue [17].

A typical hyperspectral data consists of a series of two-dimensional images, acquired at adjacent wavelengths. So, one dataset, also known as a hypercube, is a three-dimensional data set consisting of spatial or intensity information in two dimensions and spectral information in the third dimension. Since HSI requires the sample to be imaged at several contiguous wavelengths, the choice of the light source becomes important. For remote sensing of the earth [9], [10], [13], the sun provides the required broadband spectrum while in the lab or industrial settings, more specialized light sources such as Xenon arc lamp [18], [19], Mercury lamp [19], Halogen lamp [20]–[23], supercontinuum laser [24]–[26] in the visible and near-infrared

The associate editor coordinating the review of this manuscript and approving it for publication was Sukhdev Roy.

spectrum (400 nm – 2500 nm) and synchrotron radiation source [27], [28] in the mid-infrared spectrum have been used. Light-emitting diodes which are cheaper compared to other light sources have also been used to perform HSI [29]–[31] but because of their narrowband emission, several diodes centered at different wavelengths are required to cover a broadband illumination.

Hyperspectral imaging can be performed in two ways, simultaneous broadband illumination or sequential narrowband illumination of the sample. For the first method, the sample is illuminated with a broadband light source and then the data is acquired for spatial information at each point or in a line while using a spectrometer in detection, making it a whiskbroom [32]–[34] or push-broom [35]–[37] method respectively. For techniques using narrowband illumination such as based on liquid crystal [38], or acousto-optic filter [39]–[41], a narrow band light source that is used to illuminate the sample. The data is collected sequentially while changing the central wavelength of the filtered spectrum. In an acoustic-optic tunable filter (AOTF) based hyperspectral imaging source, a radio frequency (RF) acoustic wave is applied to a birefringent crystal through an attached piezoelectric transducer, which sets up a moving diffraction grating. The incident light is diffracted by the traveling acoustic wave and produces a diffracted beam at a particular wavelength, given by the phase-matching condition. The wavelength of the diffracted light can be changed by changing the applied RF frequency. The spectral resolution of the diffracted beam depends upon the acousto-optic (AO) interaction length and the difference in an ordinary and extraordinary refractive index of the crystal. Although a high spectral resolution can be achieved using the AOTF mechanism at video rates, it makes the system expensive and cumbersome with the need for RF power supply, piezo-electric transducer, and non-linear crystals, etc. In an HSI source using a liquid crystal tunable filter, the filtering mechanism is achieved by applying a multistage polarization interference filter with an added liquid-crystal waveplate in each stage, which allows one to control the retardance electronically. The inner surfaces of the liquid crystal cells are prepared in a way that the molecules have a preferred orientation parallel to the surface. When a voltage is applied across the electrodes of the liquid crystal, the molecules of the cells align towards the applied field and as a result, the retardance of the liquid crystal waveplate reduces and an electronically adjustable retardance is obtained. One may achieve the spectral resolution of the order of 10 nm using this method but it also requires a complicated filter mechanism to achieve a stable HSI source.

In yet another class of spectral imaging, which is similar to HSI and called multispectral imaging (MSI), the light from the source is filtered using a series of bandpass filters [42], [43]. In the case of bandpass filter-based MSI source, bandpass filters of different wavelengths are mounted on some mechanical or automated filter wheel and images are acquired by rotating the wheel for each filter sequentially. This is a simple and effective way of achieving MSI source, but the spectral resolution is limited to the bandwidth of the filters and several filters are needed to cover the whole imaging wavelength band. MSI has also been realized with multiple light-emitting diodes [44]. Compared to HSI, MSI does not allow to reconstruct the sample images with high spectral resolution.

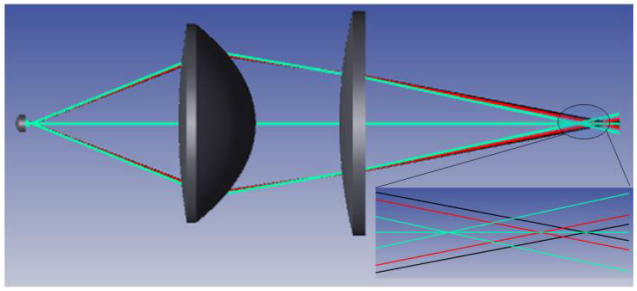

FIGURE 1. Zemax simulation of the HSI imaging system using a f = 2.7 mm focal length lens, a 0 focal length lens, and a meniscus lens for compensating the spherical aberrations. The zoom of the focal region is shown in the inset.

Recently, Chromatic confocal microscopy [45]–[47] has been demonstrated which utilizes the chromatic dispersion property of lens material to spectrally separate different wavelength components axially to enhance the imaging range of a confocal microscope. A similar methodology can be applied to a broadband laser light source such as a supercontinuum laser, to achieve a tunable hyperspectral imaging light source over a wide wavelength range. Owing to their broadband spectrum covering visible/near-infrared or mid-infrared spectrum, supercontinuum lasers have already diffused into several fields such as HSI [24]–[26], optical coherence tomography [48]–[50], chromatic confocal microscopy [46], [51], [52], fluorescence microscopy [53], [54], spectroscopy [55], [56], etc. To the best of our knowledge, the use of chromatic dispersion of lens material for the development of a hyperspectral imaging light source has not been demonstrated. In this work, using a supercontinuum laser, we designed and developed a simple yet robust HSI light source based on the chromatic dispersion property of lenses without any need for an active filter mechanism.

II. MATERIALS AND METHODS

The design of our chromatic dispersion-based hyperspectral imaging source was first simulated using a commercially available optics simulator software Optic studio (Zemax). As shown in Figure 1, the chromatic aberrations were introduced using a short focal length aspheric lens (f = 2.97 mm) and a long focal length aspheric lens (f = 32.1 mm).

The two lenses were placed at a separation of 35 mm. Although a good axial separation between different wavelength components was obtained using these two lenses, the focused spot suffered from spherical aberrations, reducing the coupling efficiency to an optical fiber. To overcome the spherical aberrations and improve the focal spot quality, we used a meniscus lens to allow tight focusing and easy

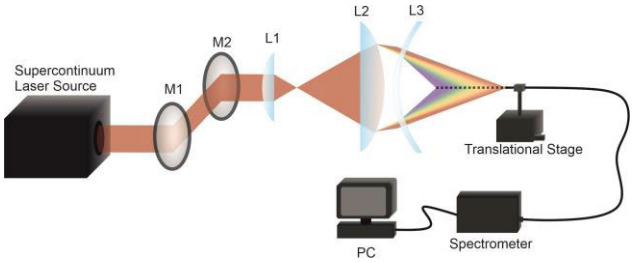

FIGURE 2. Experimental set-up for hyperspectral imaging source generation. Mirror (M1, M2), Lens (L1, L2, L3), Personal computer (PC).

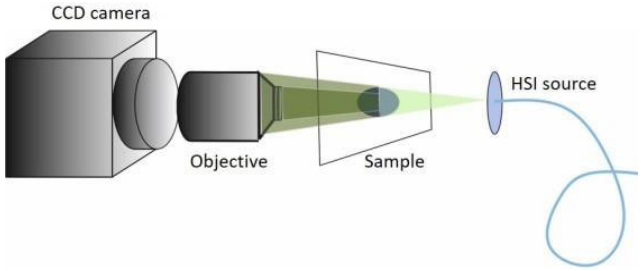

FIGURE 3. Experimental design for hypercube generation in transmission geometry.

coupling of light into an optical fiber for further applications. The meniscus lens was placed at a distance of 20 mm from the long focal length lens and the light was focused at around 58 mm behind the meniscus lens, giving enough working distance to couple light further into an optical fiber.

To experimentally apply this concept, we used a supercontinuum laser source (SCLS) (SC-OEM, YSL Photonics, China) as our primary light source because of its broadband emission from 400 nm to 2300 nm. The schematic of the experimental setup is shown in Figure 2.

The light from the SCLS is steered using mirrors M1 and M2. SCLS is a broadband light source with a wavelength ranging from 400 nm to 2300 nm. Since naturally occurring chromophores provide higher contrast in the visible-near infrared spectrum, we designed our source to cover these wavelengths only. Therefore, a dichroic mirror (M1) (DMLP900T, Thorlabs Inc., New Jersey, USA) was used as a filter to reflect the wavelengths between 400 nm and 900 nm and transmit the rest of the spectrum, which was blocked using a beam block. This reflected light from the mirror M2 was incident on a lens combination of L1 (355660-B, Thorlabs Inc. New Jersey, USA) and L2 (ACL4532U-B, Thorlabs Inc. New Jersey, USA) for introducing the chromatic aberration. A meniscus lens (LE1985-B, Thorlabs Inc. New Jersey, USA) L3 was placed 20 mm away from lens L2 for compensating the spherical aberrations. A multimode (SMF 28) fiber was mounted on a translation stage to collect the axially dispersed light where the core of the fiber worked as a pinhole. At one position of the translation stage, one wavelength band (limited by the coupling efficiency) was coupled in the fiber. The central wavelength of the coupled wavelength band could be adjusted by translating the fiber in z-direction using a translation stage translated using an actuator (Z812B, Thorlabs Inc. New Jersey, USA) with an accuracy of 29 nm. A commercial spectrometer (ATP2000P, Optosky) was used for measuring the spectrum of the HSI source, which was connected to the computer for data acquisition and further processing.

The HSI source was characterized by measuring the wavelengths coupled as a function of distance and the bandwidth of the coupled wavelengths. The capability of the HSI source was demonstrated by imaging cyan and magenta dots printed on paper. The paper was illuminated with an HSI source and the images of the dots were acquired using a CCD camera (CGE-BO13-U Mightex, Ontario, Canada) in reflection. It should be noted that, at a time, only one wavelength band centered around a certain wavelength is used to illuminate the sample. Images at different central wavelengths are acquired sequentially while translating the translational stage (Figure 1) which allows different wavelength bands to couple to the sample illumination fiber. Further, the potential of the source was tested by measuring the available fast green stained lily ovary and *hematoxylin and eosin* (H&E) stained dense connective tissue. To prepare the hypercube for these samples, we illuminated the slides at different wavelengths ranging from 490 nm to 900 nm using our hyperspectral source and imaged the sample using a 10× objective (43-907, Edmund Optics, UK) and a CCD camera (CGE-B013-U, Mightex Systems, USA), as shown in Figure 3. From the hypercube, normalized absorption was measured for the cell nucleus of the lily ovary sample as a function of wavelength. For the H&E stained dense connective tissue sample, a normalized absorption at the cell nucleus and surrounding tissue as a function of wavelength was measured.

We also imaged the lower tongue of a healthy volunteer at 540 nm, 630 nm, and white light using an endoscopic camera (B083YXRHX7, Ballylelly) with a resolution of 640 x 480 pixels. In all the experiments, we have followed our institutional policies for the use of human subjects and animals. Experiments on the lower tongue were performed as a self-test on the author of the manuscript.

III. RESULTS

The simulated result for the focal position and ray spot diagram of three different wavelength components of the light (500 nm, 700 nm, and 900 nm) as a function of distances are shown in Figure 4.

Using the chromatic aberrations of the lens combination, the 500 nm light is focused around −4.0 mm, 700 nm light at 0 mm, and the 900 nm light is focused at +4.0 mm position, giving a total separation of 8 mm approximately. A separation of 8 mm is a reasonable spectral separation of the different wavelength components to be coupled separately into an optical fiber.

We experimentally verified this simulation by traversing the translation stage and scanning the optical fiber across the Z-axis, which allowed different wavelength components to be coupled into the optical fiber, as shown in Figure 5 (a).

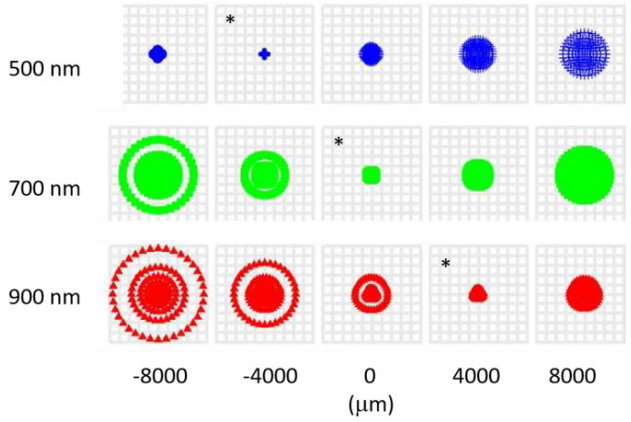

FIGURE 4. Simulated focal spot for 500 nm, 700 nm, and 900 nm as a function of distance. The focal position of the individual wavelengths is indicated by the asterisk sign.

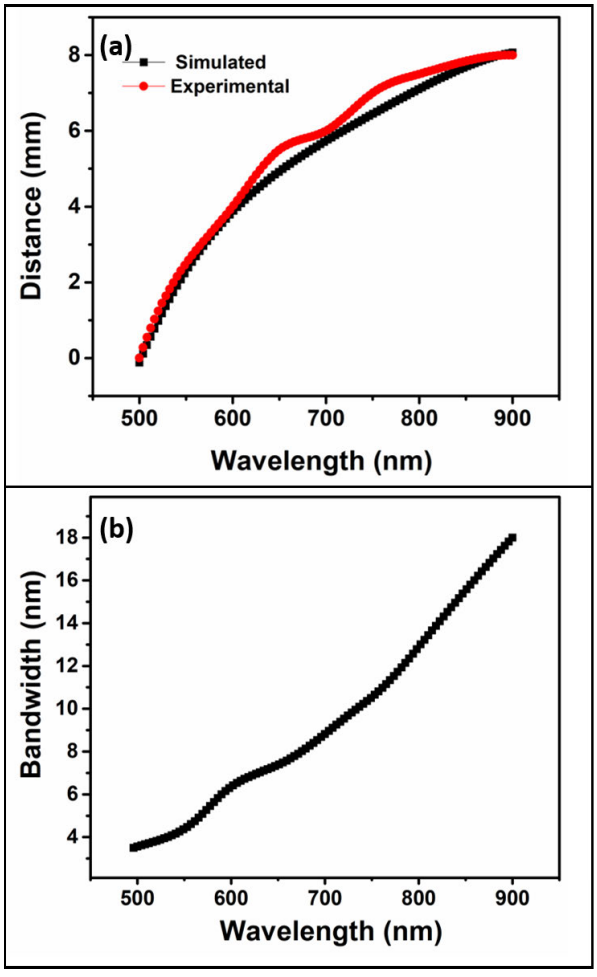

FIGURE 5. HSI source characterization. (a) Simulated and experimental data plotted between the wavelength and the focal distance. (b) The bandwidth of the coupled light measured by the spectrometer at the exit end of the optical fiber.

Experimentally, a spatial separation of 8 mm was obtained for a wavelength range of 500 nm to 900 nm (plotted in red in Figure 5 (a)), which matches well with the simulated results (plotted in black color in Figure 5 (a)). For further

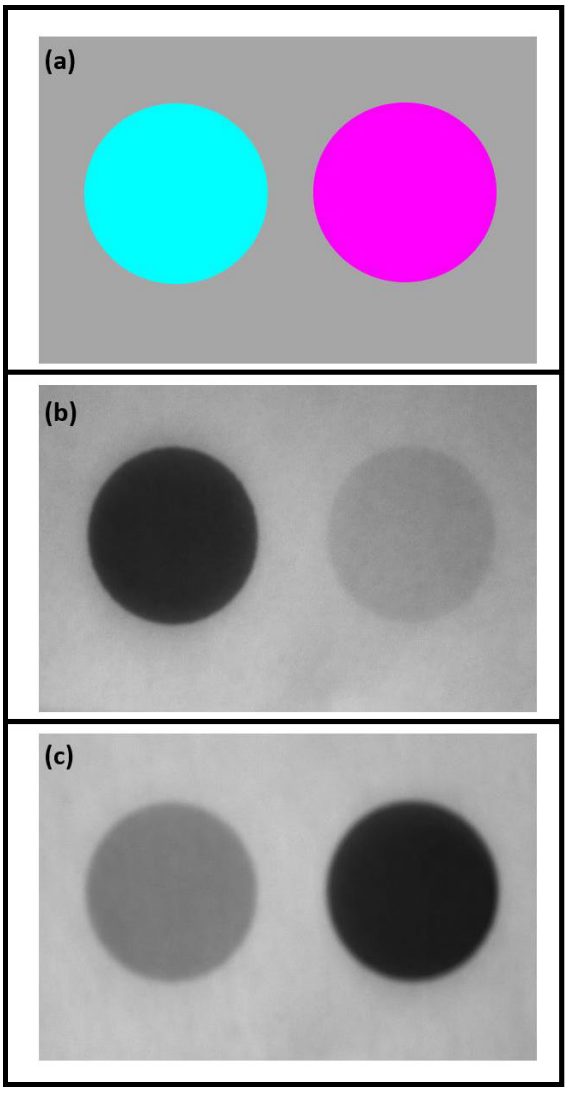

FIGURE 6. The image (a) of the cyan and magenta dots printed on a white paper illuminated with (b) 630 nm (c) 540 nm.

characterization purposes, we measured the bandwidth of the fiber-coupled light at different wavelengths using a commercial spectrometer. For the central wavelength of 500 nm, a bandwidth of 3.5 nm was measured and it increased with the increase in the central wavelength. For 900 nm central wavelength, the measured bandwidth was found to be 18 nm. The bandwidth of the coupled light to the fiber is lower for the visible wavelengths compared to the NIR wavelengths which happen because of the nonlinear chromatic dispersion of the lenses used in our system. As can be seen from Figure 5(a), visible wavelengths are focused farther apart compared to the NIR wavelengths, which leads to a narrowband coupling for visible wavelengths with respect to the NIR wavelengths.

The linear motion of the translational stage in the system allows us to continuously change the central wavelength. The precision with which the central wavelength can be changed is limited by the minimum step size of the stage movement and the stability of the laser power spectrum. For instance,

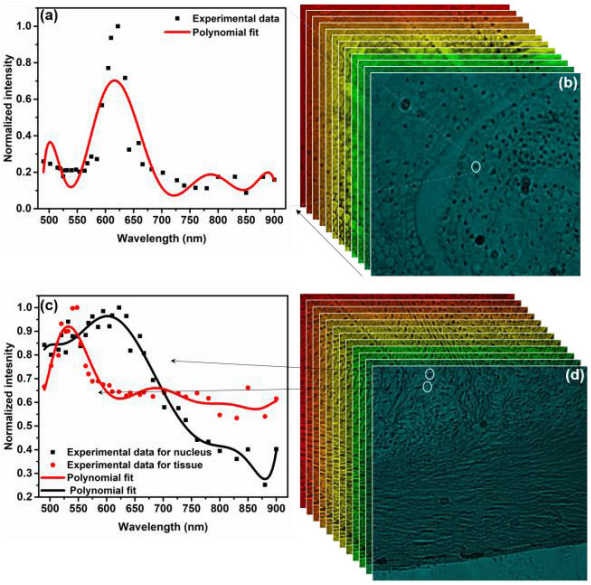

FIGURE 7. Hypercube generated using HSI for (b) Lily ovary, and (d) dense connective tissue. Normalized absorption plotted as a function wavelength measured at the locations indicated by the circle, for (a) stained cell nucleus in the lily ovary, and (c) stained cell nucleus and surrounding tissue for dense connective tissue.

in the visible range, the central wavelength changes from 500 nm to 600 nm, when the stage moves approximately by 4 mm. This corresponds to a change of approximately 0.001 nm in the central wavelength at an incremental step size of 29 nm; minimum step size of the translational stage. However our spectrometer has a resolution of 0.2 nm only, thus we could only measure the central wavelength of the light source with 0.2 nm precision. Using the translational stage and measuring with the spectrometer we were able to change the central wavelength of coupled light to the fiber with a precision of at least 0.2 nm making it an HSI source.

Once characterized, to demonstrate the applicability of the HSI source, we imaged two dots printed on a white paper with cyan and magenta inks which are routinely used in printers and known to have different reflectivity and absorption, for different wavelengths, i.e. magenta ink reflect red but absorbs green while the cyan ink reflects green but absorbs red [57]. The images of the ink dots are shown in Figure 6. As can be seen in Figure 6 (b), when illuminated with 630 nm wavelength, the magenta dot appears bright while the cyan dot appears dark because of higher absorption. Further, as can be seen in Figure 6 (c), when the illumination wavelength is changed to 540 nm, the magenta dot appears dark and the cyan dot becomes brighter.

Further to test the potential of the hyperspectral source, we generated the hypercube for fast green stained lily ovary and H&E stained dense connective tissue as shown in Figure 7 (b) and (d) respectively. The spectral signature of the cell nucleus of the lily ovary sample is shown in Figure 7 (a), where the peak absorption is around 630 nm, which is the absorption peak of the fast green dye as well [58]. For the dense connective tissue, the spectral

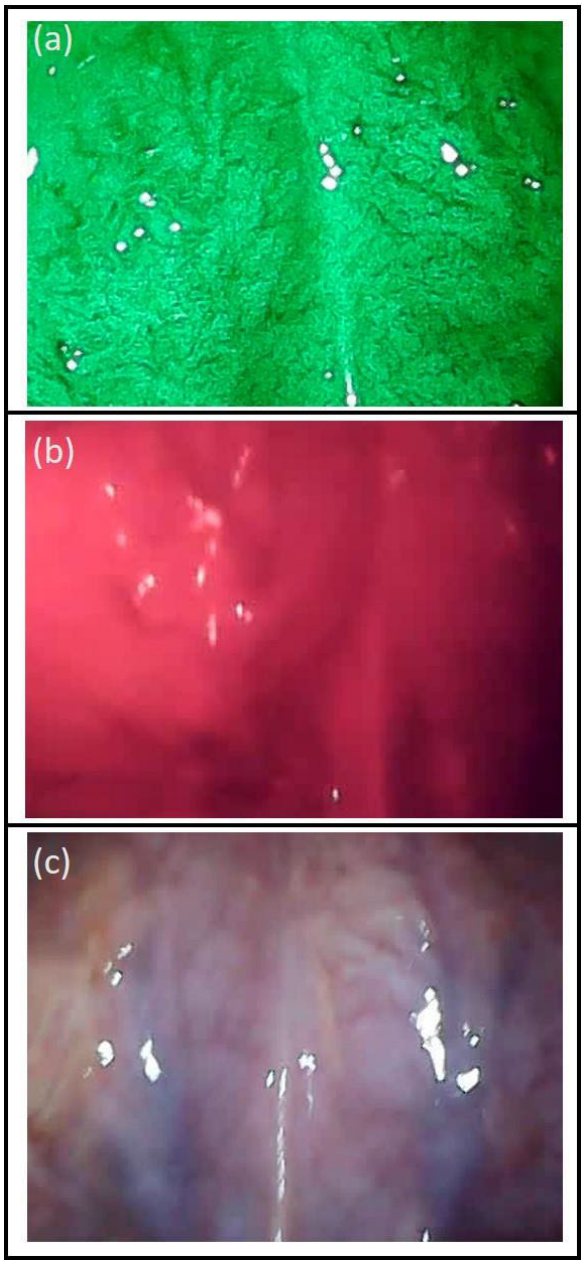

FIGURE 8. Image of the lower tongue acquired with hyperspectral source illumination using (a) 540 nm green light, (b) 630 nm red light, and (c) white light of an endoscopic camera.

signature of the cell nucleus and the surrounding tissue is shown in Figure 7 (c). For the H&E stained dense connective tissue sample, the cell nucleus stained with haematoxylin has a peak absorption around 570 nm and the surrounding tissue stained with eosin has a peak absorption at 525 nm [59], as also observed in our measurement and shown in Figure 7 (c).

The combination of the camera and the linear actuator used in our system allowed us to acquire 80 spectral images in 4 seconds.

We also imaged the lower tongue of a healthy volunteer for two different wavelengths and also with a white light

source. In Figure 8, we show the images of the lower tongue imaged under the illumination of 540 nm, 630 nm, and white light. One can see the improved contrast for blood vessels (Figure 8 (a)) which appears black at 540 nm illumination due to the high absorption of this wavelength by blood compared to the image acquired at 630 nm illumination (Figure 8 (b)). The white light image (Figure 8(c)) does provide some contrast for the blood vessels but still inferior to the imaging under 540 nm illumination.

IV. DISCUSSION AND CONCLUSION

The bandwidth of our developed HSI light source which defines the spectral resolution of the HSI system is relatively wider at higher wavelengths compared to the bandwidth at the lower wavelengths. This however is still considerably lower than other available HSI light sources based on liquid crystal tunable filter (LCTF). For instance, a commercial HSI source reaches a bandwidth of $\sim$20 nm, which is almost two times that of ours at 730 nm (10 nm). The spectral resolution of the fiber-coupled HSI source can be further improved by using smaller core diameter fiber compared to SMF 28. The increase in resolution will be at the expense of the coupled power due to the smaller core diameter. Moreover, the use of smaller core fiber will limit the coupling of the higher wavelength components, therefore SMF 28 multimode fiber is an optimum choice compared to a single-mode fiber.

One challenge common to all HSI light sources is that the power transmitted by the supercontinuum laser is not uniform as a function of wavelength. Usually, supercontinuum light sources have more power around 800 nm compared to 400 nm, and one needs to calibrate the filter to take illumination power independent images. This is the case with our HSI system as well but it can be easily handled by proper post-processing calibration. One may take a reference signal at all the wavelengths using a mirror and recalibrate the measured data in post-processing.

The sweeping time of different wavelengths is another aspect to be considered for an HSI source. The response time of the tunable filters used in HSI sources is generally fast. The LCTFs take milliseconds to switch between wavelengths and AOTFs have a microsecond response time. In our case we are using an automated linear translation stage, which takes approximately 4 seconds to travel 8 mm distance, making the wavelength tuning slower compared to other sources. This can however be improved using fast linear translation stages.

In conclusion, we have designed and developed a wide tunable fiber-coupled hyperspectral imaging light source based on the chromatic dispersion property of the off-the-shelf lenses. Using three lenses, we achieved a total spectral separation of 8 mm for the light from 490 nm to 900 nm. We could easily couple these axially separated wavelength bands in a multimode optical fiber for imaging purposes. The bandwidth of our HSI source ranges from 3.4 nm at 490 nm to 18 nm at 900 nm respectively, which is more than two times better than the commercially available HSI sources. The potential of the HSI source was demonstrated by imaging two dyes with an absorption band at two different wavelengths and generating hypercubes for lily ovary and dense connective tissue, demonstrating the capability of the HSI source to detect different chemicals having absorption bands at different wavelengths.

We also imaged the lower tongue of a healthy volunteer at two wavelengths (540 nm and 630 nm) and white light, and could distinctly see the difference in contrast. The vascularization of the lower tongue is more visible at 540 nm compared to 630 nm or white light image. We believe that our simple design can be easily combined with a supercontinuum light source and convert it into an HSI source. Being a fiber-coupled source, it can be easily incorporated into a standard endoscope or microscope for hyperspectral imaging.

REFERENCES

[1] A. J. M. Wollman, R. Nudd, E. G. Hedlund, and M. C. Leake, "From Animaculum to single molecules: 300 years of the light microscope," *Open Biol.*, vol. 5, no. 4, Apr. 2015, Art. no. 150019.

[2] K. Kuznetsov, R. Lambert, and J.-F. Rey, "Narrow-band imaging: Potential and limitations," *Endoscopy*, vol. 38, no. 1, pp. 76–81, Jan. 2006.

[3] S. W. Wilkins, T. E. Gureyev, D. Gao, A. Pogany, and A. W. Stevenson, "Phase-contrast imaging using polychromatic hard X-rays," *Nature*, vol. 384, no. 6607, pp. 335–338, Nov. 1996.

[4] D. Huang, E. A. Swanson, C. P. Lin, J. S. Schuman, W. G. Stinson, W. Chang, M. R. Hee,T. Flotte, K. Gregory, and C. A. Puliafito, "Optical coherence tomography," *Science*, vol. 254, no. 5035, p. 1178, 1991.

[5] W. A. Kalender, "X-ray computed tomography," *Phys. Med. Biol.*, vol. 51, no. 13, pp. R29–R43, Jun. 2006.

[6] M. F. Reiser, W. Semmler, and H. Hricak, *Magnetic Resonance Tomography*. Berlin, Germany: Springer-Verlag, 2007.

[7] P. Davidovits and M. D. Egger, "Scanning laser microscope," *Nature*, vol. 223, no. 5208, p. 831, Aug. 1969.

[8] J. W. Lichtman and J.-A. Conchello, "Fluorescence microscopy," *Nature Methods*, vol. 2, no. 12, pp. 910–919, Dec. 2005.

[9] J. Nieke, K. I. Itten, and W. Debryun, "The airborne imaging spectrometer APEX: From concept to realisation," in *Proc. 4th EARSeL Workshop Imag. Spectrosc.*, 2005, pp. 73–80.

[10] A. F. H. Goetz, G. Vane, J. E. Solomon, and B. N. Rock, "Imaging spectrometry for earth remote sensing," *Science*, vol. 228, no. 4704, pp. 1147–1153, 1985.

[11] B. Zhang, D. Wu, L. Zhang, Q. Jiao, and Q. Li, "Application of hyperspectral remote sensing for environment monitoring in mining areas," *Environ. Earth Sci.*, vol. 65, no. 3, pp. 649–658, Feb. 2012.

[12] A. A. Gowen, C. P. O'Donnell, P. J. Cullen, G. Downey, and J. M. Frias, "Hyperspectral imaging–an emerging process analytical tool for food quality and safety control," *Trends Food Sci. Technol.*, vol. 18, no. 12, pp. 590–598, Dec. 2007.

[13] T. Adão, J. Hruška, L. Pádua, J. Bessa, E. Peres, R. Morais, and J. Sousa, "Hyperspectral imaging: A review on UAV-based sensors, data processing and applications for agriculture and forestry," *Remote Sens.*, vol. 9, no. 11, p. 1110, Oct. 2017.

[14] E. K. Hege, O. C. Dan, J. William, B. Shridhar, and L. D. Eustace, "Hyperspectral imaging for astronomy and space surveillance," *Proc. SPIE*, vol. 5159, pp. 380–391, Jan. 2004.

[15] J. Ren, J. Zabalza, S. Marshall, and J. Zheng, "Effective feature extraction and data reduction in remote sensing using hyperspectral imaging [applications corner]," *IEEE Signal Process. Mag.*, vol. 31, no. 4, pp. 149–154, Jul. 2014.

[16] C. Cucci, J. K. Delaney, and M. Picollo, "Reflectance hyperspectral imaging for investigation of works of art: Old master paintings and illuminated manuscripts," *Accounts Chem. Res.*, vol. 49, no. 10, pp. 2070–2079, Oct. 2016.

[17] G. Lu and B. Fei, "Medical hyperspectral imaging: A review," *J. Biomed. Opt.*, vol. 19, no. 1, pp. 1–24, Jan. 2014.
[18] H. Akbari, L. Halig, D. M. Schuster, B. Fei, A. Osunkoya, V. Master, P. Nieh, and G. Chen, "Hyperspectral imaging and quantitative analysis for prostate cancer detection," *J. Biomed. Opt.*, vol. 17, no. 7, Jul. 2012, Art. no. 076005.
[19] R. A. Schultz, T. Nielsen, J. R. Zavaleta, R. Ruch, R. Wyatt, and H. R. Garner, "Hyperspectral imaging: A novel approach for microscopic analysis," *Cytometry*, vol. 43, no. 4, pp. 239–247, Apr. 2001.
[20] P. M. Mehl, Y.-R. Chen, M. S. Kim, and D. E. Chan, "Development of hyperspectral imaging technique for the detection of apple surface defects and contaminations," *J. Food Eng.*, vol. 61, no. 1, pp. 67–81, Jan. 2004.
[21] G. ElMasry, N. Wang, A. ElSayed, and M. Ngadi, "Hyperspectral imaging for nondestructive determination of some quality attributes for strawberry," *J. Food Eng.*, vol. 81, no. 1, pp. 98–107, Jul. 2007.
[22] J. Qiao, M. O. Ngadi, N. Wang, C. Gariépy, and S. O. Prasher, "Pork quality and marbling level assessment using a hyperspectral imaging system," *J. Food Eng.*, vol. 83, no. 1, pp. 10–16, Nov. 2007.
[23] H. Akbari, K. Uto, Y. Kosugi, K. Kojima, and N. Tanaka, "Cancer detection using infrared hyperspectral imaging," *Cancer Sci.*, vol. 102, no. 4, pp. 852–857, Apr. 2011.
[24] Z. Guo, Y. Liu, X. Zheng, and K. Yin, "Active hyperspectral imaging with a supercontinuum laser source in the dark," *Chin. Phys. B*, vol. 28, no. 3, Mar. 2019, Art. no. 034206.
[25] O. H. A. Nielsen, A. L. Dahl, R. Larsen, F. Møller, F. D. Nielsen, C. L. Thomsen, H. Aanæs, and J. M. Carstensen, "Supercontinuum light sources for hyperspectral subsurface laser scattering," in *Image Analysis*, Berlin, Germany: Springer, 2011, pp. 327–337.
[26] M. Torabzadeh, P. A. Stockton, G. T. Kennedy, R. B. Saager, A. J. Durkin, R. A. Bartels, and B. J. Tromberg, "Hyperspectral imaging in the spatial frequency domain with a supercontinuum source," *J. Biomed. Opt.*, vol. 24, no. 7, Jul. 2019, Art. no. 071614.
[27] M. K. Kuimova, K. L. A. Chan, and S. G. Kazarian, "Chemical imaging of live cancer cells in the natural aqueous environment," *Appl. Spectrosc.*, vol. 63, no. 2, pp. 164–171, Feb. 2009.
[28] H.-Y.-N. Holman, R. Miles, Z. Hao, E. Wozei, L. M. Anderson, and H. Yang, "Real-time chemical imaging of bacterial activity in biofilms using open-channel microfluidics and synchrotron FTIR spectromicroscopy," *Anal. Chem.*, vol. 81, no. 20, pp. 8564–8570, Oct. 2009.
[29] H. Wang, Y. Hu, X. Ma, J. Sun, X. Sun, D. Chen, X. Zheng, and Q. Li, "An active hyperspectral imaging system based on a multi-LED light source," *Rev. Sci. Instrum.*, vol. 90, no. 2, Feb. 2019, Art. no. 026107.
[30] T. Heimpold, F. Reifegerste, S. Drechsel, and J. Lienig, "LED for hyperspectral imaging—A new selection method," *Biomed. Eng.*, vol. 63, no. 5, pp. 529–535, Oct. 2018.
[31] K. Islam, M. Ploschner, and E. M. Goldys, "Multi-LED light source for hyperspectral imaging," *Opt. Exp.*, vol. 25, no. 26, pp. 32659–32668, 2017.
[32] J. E. Fowler, "Compressive pushbroom and whiskbroom sensing for hyperspectral remote-sensing imaging," in *Proc. IEEE Int. Conf. Image Process. (ICIP)*, Oct. 2014, pp. 684–688.
[33] K. Uto, H. Seki, G. Saito, Y. Kosugi, and T. Komatsu, "Development of a low-cost hyperspectral whiskbroom imager using an optical fiber bundle, a swing mirror, and compact spectrometers," *IEEE J. Sel. Topics Appl. Earth Observ. Remote Sens.*, vol. 9, no. 9, pp. 3909–3925, Sep. 2016.
[34] L. Qingli, H. Xiaofu, W. Yiting, L. Hongying, X. Dongrong, and G. Fangmin, "Review of spectral imaging technology in biomedical engineering: Achievements and challenges," *J. Biomed. Opt.*, vol. 18, pp. 1–29, Oct. 2013.
[35] H.-T. Lim and V. M. Murukeshan, "Pushbroom hyperspectral imaging system with selectable region of interest for medical imaging," *J. Biomed. Opt.*, vol. 20, no. 4, Apr. 2015, Art. no. 046010.
[36] R. Arablouei, E. Goan, S. Gensemer, and B. Kusy, "Fast and robust pushbroom hyperspectral imaging via DMD-based scanning," *Proc. SPIE*, vol. 9948, Sep. 2016, Art. no. 99480A.
[37] K. C. Lawrence, B. Park, W. R. Windham, and C. Mao, "Calibration of a pushbroom hyperspectral imaging system for agricultural inspection," *Trans. ASAE*, vol. 46, no. 2, p. 513, 2003.
[38] R. W. Slawson, Z. Ninkov, and E. P. Horch, "Hyperspectral imaging: Wide-area spectrophotometry using a liquid-crystal tunable filter," *Publications Astronomical Soc. Pacific*, vol. 111, no. 759, pp. 621–626, May 1999.
[39] N. Gupta, R. Dahmani, M. S. Gottlieb, L. J. Denes, B. Kaminsky, and P. Metes, "Hyperspectral imaging using acousto-optic tunable filters," *Proc. SPIE*, vol. 3718, Aug. 1999, pp. 512–521.
[40] N. Gupta and V. Voloshinov, "Hyperspectral imager, from ultraviolet to visible, with a KDP acousto-optic tunable filter," *Appl. Opt.*, vol. 43, no. 13, pp. 2752–2759, May 2004.
[41] B. Park, S. C. Yoon, S. Lee, J. Sundaram, W. R. Windham, A. Hinton, Jr., and K. C. Lawrence, "Acousto-optic tunable filter hyperspectral microscope imaging method for characterizing spectra from food-borne pathogens," *Trans. ASABE*, vol. 55, no. 5, pp. 1997–2006, 2012.
[42] G. Themelis, J. S. Yoo, and V. Ntziachristos, "Multispectral imaging using multiple-bandpass filters," *Opt. Lett.*, vol. 33, no. 9, pp. 1023–1025, 2008.
[43] A. Pelagotti, A. Mastio, A. Rosa, and A. Piva, "Multispectral imaging of paintings," *IEEE Signal Process. Mag.*, vol. 25, no. 4, pp. 27–36, Jul. 2008.
[44] J.-I. Park, M.-H. Lee, M. D. Grossberg, and S. K. Nayar, "Multispectral imaging using multiplexed illumination," in *Proc. IEEE 11th Int. Conf. Comput. Vis.*, Oct. 2007, pp. 1–8.
[45] H. J. Tiziani and H.-M. Uhde, "Three-dimensional image sensing by chromatic confocal microscopy," *Appl. Opt.*, vol. 33, no. 10, pp. 1838–1843, 1994.
[46] K. Shi, P. Li, S. Yin, and Z. Liu, "Chromatic confocal microscopy using supercontinuum light," *Opt. Exp.*, vol. 12, no. 10, pp. 2096–2101, 2004.
[47] A. Ramy, S. Samir, H. Joseph, and F. Qiyin, "Hyperspectral imaging: Comparison of acousto-optic and liquid crystal tunable filters," *Proc. SPIE*, vol. 10573, Mar. 2018, Art. no. 105732P.
[48] Y. Wang, Y. Zhao, J. S. Nelson, Z. Chen, and R. S. Windeler, "Ultrahigh-resolution optical coherence tomography by broadband continuum generation from a photonic crystal fiber," *Opt. Lett.*, vol. 28, no. 3, pp. 182–184, Feb. 2003.
[49] J. A. Gardecki, K. Singh, C.-L. Wu, and G. J. Tearney, "Imaging the human prostate gland using 1-μm-resolution optical coherence tomography," *Arch. Pathol. Lab. Med.*, vol. 143, no. 3, pp. 314–318, 2019.
[50] N. Nishizawa, Y. Chen, P. Hsiung, E. Ippen, and J. Fujimoto, "Real-time, ultrahigh-resolution, optical coherence tomography with an all-fiber, femtosecond fiber laser continuum at 1.5 μm," *Opt. Lett.*, vol. 29, no. 24, pp. 2846–2848, 2004.
[51] C. Olsovsky, R. Shelton, O. Carrasco-Zevallos, B. E. Applegate, and K. C. Maitland, "Chromatic confocal microscopy for multi-depth imaging of epithelial tissue," *Biomed. Opt. Exp.*, vol. 4, no. 5, pp. 732–740, 2013.
[52] U. Minoni, G. Manili, S. Bettoni, E. Varrenti, D. Modotto, and C. De Angelis, "Chromatic confocal setup for displacement measurement using a supercontinuum light source," *Opt. Laser Technol.*, vol. 49, pp. 91–94, Jul. 2013.
[53] D. Wildanger, E. Rittweger, L. Kastrup, and S. W. Hell, "STED microscopy with a supercontinuum laser source," *Opt. Exp.*, vol. 16, no. 13, pp. 9614–9621, 2008.
[54] C. Poudel and C. F. Kaminski, "Supercontinuum radiation in fluorescence microscopy and biomedical imaging applications," *J. Opt. Soc. Amer. B, Opt. Phys.*, vol. 36, no. 2, pp. A139–A153, 2019.
[55] J. Kilgus, K. Duswald, G. Langer, and M. Brandstetter, "Mid-infrared standoff spectroscopy using a supercontinuum laser with compact Fabry–Pérot filter spectrometers," *Appl. Spectrosc.*, vol. 72, no. 4, pp. 634–642, 2018.
[56] M. K. Dasa, C. Markos, M. Maria, C. R. Petersen, P. M. Moselund, and O. Bang, "High-pulse energy supercontinuum laser for high-resolution spectroscopic photoacoustic imaging of lipids in the 1650-1850 nm region," *Biomed. Opt. Exp.*, vol. 9, no. 4, pp. 1762–1770, 2018.
[57] H. Mathieu and D. H. Roger, "Deducing ink-transmittance spectra from reflectance and transmittance measurements of prints," *Proc. SPIE*, vol. 6493, Jan. 2007, Art. no. 649314.
[58] M. H. Werts, V. Raimbault, R. Texier-Picard, R. Poizat, O. Français, L. Griscom, and J. R. Navarro, "Quantitative full-colour transmitted light microscopy and dyes for concentration mapping and measurement of diffusion coefficients in microfluidic architectures," *Lab Chip*, vol. 124, pp. 808–820, 2012.
[59] S. L. Gibbs, E. Genega, J. Salemi, V. Kianzad, H. L. Goodwill, Y. Xie, R. Oketokoun, P. Khurd, A. Kamen, and J. V. Frangioni, "Near-infrared fluorescent digital pathology for the automation of disease diagnosis and biomarker assessment," *Mol. Imag.*, vol. 14, no. 5, pp. 1–9, 2015.

GARGI SHARMA received the Ph.D. degree from the National Institute of Scientific Research, Canada, in 2013. She was a Postdoctoral Fellow with the Harvard Medical School, USA, until 2018. She is currently a Postdoctoral Fellow with the Max Planck Institute for the Physics of Light, Germany. Her current research interests include the development of novel miniaturized devices for optical coherence tomography and thermographic imaging.

SHEEZA KAINAT NAVEED is currently pursuing the Master of Physics degree with the Friedrich-Alexander Universität Erlangen-Nürnberg, Germany.

ASHA PARMAR received the master's degree from Maharshi Dayanand University, Rohtak, India. She is currently pursuing the Ph.D. degree with the Max Planck Institute for the Science of Light, Erlangen, Germany.

KANWARPAL SINGH received the Ph.D. degree from the National Institute of Scientific Research, Canada, in 2013. He was a Postdoctoral Fellow with the Harvard Medical School, USA, until 2018, where he worked on the development of high-resolution optical coherence tomography systems. He currently leads an independent research group (Microendoscopy) at the Max Planck Institute for the Science of Light, Erlangen, Germany. His research group focuses on the development of miniaturized flexible endoscopic devices for imaging inside the body.